AE Source Localization in a Steel Plate with the Dispersive A_0 Mode based on the Cross-Correlation Technique and Time Reversal Principle

by Zenghua Liu*, Tuocan Dong†, Qiuling Peng†, Cunfu He†, Qiufeng Li‡, and Bin Wu†

ABSTRACT

The accuracy of damage localization, especially the accurate determination of the time arrival difference, is important in the field of acoustic emission (AE) source localization. In this paper, we propose a new approach to localize an AE source with the dispersive A_0 mode. For this approach, we analyzed the cross correlation of AE signals with a reference database and determined the time lag of A_0 mode. The technique is carried out in a two-stage computational process. First, AE signals are used to construct the reference database and compensate for the dispersion of waves based on the time reversal principle. Second, the time arrival difference of the A_0 mode is determined by the cross correlation of AE signals with the reference signals using the first threshold-crossing technique. A localization algorithm is carried out based on the triangulation technique. The proposed approach is conducted on a steel plate with three AE sensors coupling on the surface. Pencil-lead breaks are adopted to simulate AE sources. Results indicated that eight verification points were successfully localized with the maximum and minimum relative errors of 0.98% and 0.58%, respectively. Thus, this paper shows an optional technique to localize AE sources with the A_0 mode, which is of significant importance.

KEYWORDS: acoustic emission, source localization, time reversal, cross correlation, pencil-lead break

Introduction

Various techniques have been developed to guarantee the safety and operational performance of different structures, such as composite parts (Liu et al., 2013b), aircrafts (Han et al., 2011), bridges (Pullin et al., 1999), pipelines (Liu et al., 2015b), and concrete materials (Grondel et al., 2002; Li et al., 2015). Among the various techniques used for structural health monitoring (SHM), the acoustic emission (AE) method is widely used to evaluate and investigate damage positions in structures. AE is a mechanical stress wave resulting from an energy released during microstructural changes. The waves travel through structures and lead to micro displacement on the structure's surface, which can be detected by AE sensors (Wevers, 1997). In general, AE waves show characteristics of lamb waves when propagating in plate-like structures. Researchers have investigated the applications of lamb waves for several years because it is a promising candidate in monitoring and evaluating damages (Liu et al., 2013a; Niri and Salamone, 2012). However, this technique still has some disadvantages because of its multimode and dispersive characteristics (Barthorpe et al., 2012; Harb and Yuan, 2015). AE source localization using lamb waves can be achieved by using an active-passive or passive only approach (Niri and Salamone, 2012). In the active-passive approach, both emitting and receiving transducers are used, whereas in the passive approach, only receiving transducers are used. The AE technique is a typical passive technique in which only receiving transducers are used. In large plate-like structures, two fundamental lamb wave modes always exist: symmetric mode (S mode) and antisymmetric mode (A mode), which

* College of Mechanical Engineering and Applied Electronics Technology, Beijing University of Technology, Beijing, 100124, China; email: liuzenghua@bjut.edu.cn
† College of Mechanical Engineering and Applied Electronics Technology, Beijing University of Technology, Beijing, 100124, China
‡ The Ministry of Education Key Laboratory of NDT, Nanchang Hangkong University, Nanchang, 330063, China

have different types of vibration displacements and travel at different frequencies. Figure 1 shows the mode shapes of two lamb waves in plate-like structures (Watkins and Jha, 2012).

Figure 2 shows group velocity dispersion curves of lamb waves in a 3 mm thick steel plate. Here, its longitudinal wave velocity is 5960 m/s, its shear wave velocity is 3260 m/s, and its density is 7932 kg/m^3. The dispersion curves illustrate that the different frequency components of lamb waves travel at different velocities. The nature of lamb wave modes leads to a drastic decrease in the performance of a source localization system (Ciampa and Meo, 2010). In the low-frequency range (<200 kHz), only A_0 and S_0 modes exist. The S_0 mode travels faster than the A_0 mode and shows a nondispersive characteristic, whereas the A_0 mode is largely dispersive. The dispersion characteristic makes it difficult to analyze the arrival times when localizing AE sources based on the A_0 mode. However, in large plate-like structures, due to the attenuation effect, a low-frequency A_0 mode can propagate a long distance with high energy (Ziola and Gorman, 1991; He et al., 2017), which indicates that the A_0 mode of lamb waves has a promising application in AE source localization.

A classical way to localize the AE source is to calculate the distance between the source and the sensor by the multiplication of wave velocity with the arrival time of waves. This technique is commonly used in the AE method for its ability to locate the source (Kishi et al., 1991), but it is impossible to obtain the arrival time of waves because the exact time of generation of acoustic events is unknown (Kundu, 2014). Therefore, a modified approach of source localization was developed based on the arrival time difference technique. The arrival time difference is the difference of arrival times or the arrival time delay among different sensors (Aljet et al., 2012; Xiao et al., 2014). This approach is always applied to the sensor array by measuring the velocity of AE waves and the arrival time difference. This approach is applicable to isotropic materials, such as metallic materials. However, uncertainties are inevitably introduced into the arrival time difference measurement because of random errors, systematic errors, and AE signal characteristics (multimode and dispersion). To reduce these errors, different techniques have been investigated to determine the arrival time difference.

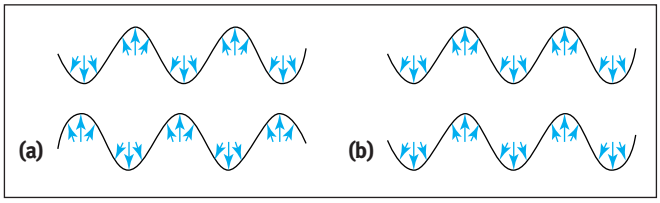

Figure 1. Two lamb waves mode shapes in plate-like structures: (a) symmetric lamb waves mode; (b) antisymmetric lamb waves mode.

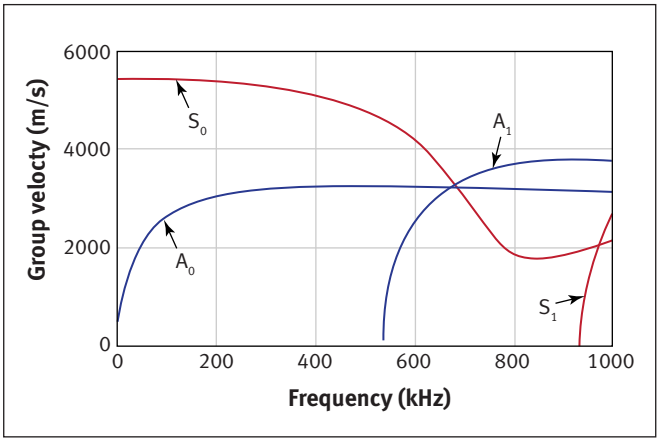

Figure 2. Group velocity dispersion curves of lamb wave in a 3 mm thick steel plate.

In previous research, other authors (Sedlak et al., 2013) presented an automatic determination technique for the first arrival time based on the akaike information criterion (AIC) of AE signals for a thin multilayer plate. In the study, the first-coming mode (S_0 mode) was not dispersive due to the short source-to-sensor distance and the small plate-like specimens used. Although it is still difficult to quantify the reliability of the arrival time, the proposed two-step AIC approach is a useful tool to locate AE events by automatically assigning arrival time. However, in large plate-like structures, dispersion and multimode nature are two crucial factors in AE event localization. To minimize the influence of multimode nature and dispersion, other authors (Mohd et al., 2014) proposed a novel technique of wavelet transform analysis and modal location based on lamb waves theory and time-frequency analysis and proved that this technique is more accurate for source localization than the time of arrival (TOA) technique. Also, it could be considered a more reliable and easier source localization methodology than delta T, since no test grid and Hsu-Nielsen source for training data is needed.

Other authors (Zarate et al., 2015) proposed a bayesian framework that considered uncertainties in wave velocities and arrival times and adopted a continuous wavelet transform (CWT) to calculate. They obtained a greater accuracy with the use of liquid-borne waves and obtained reliability through the bayesian approach, which can eventually lead to significant improvements in source localization technology for liquid-filled tanks. Other authors (Niri and Salamone, 2012) proposed a probabilistic approach for AE source localization in an isotropic plate based on an extended kalman filter (EKF) and studied the uncertainties by using the CWT technique. Further research (Zhong et al., 2015) achieved multi-impact localization on aircraft composite structures by using the near-field two-dimensional (2D) multiple signal classification (2D-MUSIC) algorithm and a uniform linear PZT sensor array. Moreover, many researchers have investigated various signal-processing techniques, such as the time-frequency analysis (Kishimoto et al., 1995; Poggi et al., 2013), the wavelet analysis (Mostafapour and Davoodi, 2015;

Poggi et al., 2013), the time reversal technique (Liu et al., 2014; Liu et al., 2015a; Draeger and Fink, 1999; Draeger et al., 1999; Sohn et al., 2007), and the cross-correlation technique (Chen et al., 2012; Kim et al., 2015).

Among these techniques, the cross-correlation technique shows the possibility of determining the time delay of signals. Cross correlation is one of the signal-processing techniques used to compare the similarity between two different signals as a function of time lag. In most of the cases, the obtained sensor outputs were compared with the reference database signal, and then the similarity or time lag was identified. Other research (Kim et al., 2015) improved a normalized cross-correlation technique to localize the low-velocity impact position in a stiffened composite panel. It showed that the proposed technique more accurately estimated the actual location of the impact source by comparing the normalized cross-correlation between the reference database and the obtained impact signals. Other authors (Ziola and Gorman, 1991) determined the arrival time difference by cross-correlating the output signal obtained from the AE sensors with a single frequency cosine wave modulated by a gaussian pulse. The idea behind this research is that if a single frequency in the AE signal can be isolated, then the arrival time differences due to the propagation of that frequency component can be used for the location analysis. Generally, in the cross-correlation technique, a pre-obtained reference database is essential. Many techniques can be chosen to construct the reference signal, such as simulating a modulated signal or training points for the monitoring structure. However, the training process of points is time-consuming due to many prior preliminary works before the experiment. In this study, the reference signal was constructed with the AE signals obtained from different sensors based on the time reversal technique, which saves time. The time reversal technique has been widely used to evaluate impacts or defects on plate-like structures (Liu et al., 2011; Chen et al., 2011; He and Yuan, 2016). It can make a signal more visible with a high resolution in time domain because of its functions of inverse filtering (Ciampa and Meo, 2011), dispersion compensation (Ernst and Dual, 2014), signal self-focus (Ing and Fink, 1998), signal reconstruction (Mustapha et al., 2014), and multichannel signal focusing (Liu et al., 2014).

In this research, we combined the advantages of three techniques, including time reversal, CWT, and cross correlation, to analyze AE signals. The time reversal technique was chosen to construct the reference signal, compensating for the dispersion and improving the signal-to-noise ratio of the focused waveform. The CWT technique was used to extract a narrowband component of the AE signal, as the AE signal is a broadband signal. The reference signal was narrowband and the dispersion was compensated after time reversal, and then it was used to determine the arrival time difference of the A_0 mode based on the cross-correlation technique. Some related techniques used in the literature are summarized in Table 1.

This paper is organized as follows. First, the arrival time difference is used to localize the position of the AE sources. In a large plate, AE source localization can be simplified as a two-dimensional source localization model using the triangulation technique (Kaphle, 2012a).

Second, we explain the reference signal construction based on CWT and the time reversal technique. Next, we show the experimental setup and compare the localization results of the proposed technique with the first threshold-crossing technique. Some conclusions of the proposed technique are presented in the conclusions.

Reference Signal Construction

In this study, the reference signal was captured by the AE sensor. The time difference Δt can be obtained by cross correlating different AE signals with the reference signal (Ziola and Gorman, 1991; Kim et al., 2015). As described above, the reference signal is necessary and important when conducting cross correlation with AE signals. Many techniques can be used to construct the reference signal to

TABLE 1
Related techniques used in literature review

Citations	Techniques used*			Key words of functions
	TR	CWT	CC	
Chen et al., 2011; Liu et al., 2011; He and Yuan, 2016; Ciampa and Meo, 2011	X			Signal focusing
Chen et al., 2011; Liu et al., 2011; He and Yuan, 2016; Ciampa and Meo, 2011	X			Dispersion compensation
Mustapha et al., 2014	X			Signal reconstruction
Mustapha et al., 2014		X		Signal filtering
Zarate et al., 2015		X		Uncertainty element
Mostafapour and Davoodi, 2015		X		Frequency selection
Ziola and Gorman, 1991			X	Time-lag calculation
Kim et al., 2015			X	Impact source localization

* TR = Time reverse; CWT = Continuous wavelet transform; CC = Cross correlation

compare the similarity of two signals or calculate the arrival time difference. In this study, to obtain the reference signal, two steps have been carried out. The first step is to extract the narrowband component from the AE signals. In other words, the dominant frequency component should be isolated from the AE signals. The second step is to focus the narrowband signal in time domain based on the time reversal principle. Consequently, the focused signal serves as the reference signal. In general, narrowband component extraction is achieved by the CWT technique due to its abundant information and high resolutions both in time and frequency domains. The extracted narrowband signals were then time reversed and focused with the improved signal-to-noise ratio.

Narrowband Component Extraction

The wavelets have the maximum resolutions in time and frequency, which are dependent on the mother wavelet. Different mother wavelets have been investigated (Niri and Salamone, 2012; Mohd et al., 2014), and the morlet wavelet was chosen and applied in AE due to its admissibility as a wavelet of a zero mean value (Zitto et al., 2015).

The complex morlet wavelet is defined as:

$$\psi(t)=\frac{1}{\sqrt{\pi f_b}}e^{-\frac{t^2}{f_b}}e^{2\pi f_c jt} \quad (1)$$

where

f_b and f_c, respectively, represent the bandwidth frequency and the center frequency,
π is the ratio of circumference to diameter,
e is the Euler's number,
j is the imaginary unit.

After a signal is transformed by CWT, the information can be determined from CWT both in time and frequency domains. As the X vector is time and the Y vector is frequency, the numeric values in the continuous wavelet transform matrix represent the wavelet coefficients. The dominant frequency of the AE signal can be obtained by fast fourier transform (FFT). The dominant frequency component is extracted from the wavelet scale matrix according to the relationship between wavelet scale and the frequency:

$$f_a=\frac{f_c}{a}T_s \quad (2)$$

where

f_a is the extracted frequency,
T_s is the sampling interval of AE signals.

In actual operation, the extracted frequency f_a is not single but narrowband.

Reference Signal Construction based on Time Reversal Principle

The second step to construct the reference signal is to focus on the extracted signal in the time domain based on the time reversal principle. In many signal-processing applications, time reversal acts as a spatiotemporal matched filter to compensate for the shift of signal (Tanter et al., 2000). However, it is discovered that narrowband signals behave better than broadband signals in minimizing amplitude dispersion (Park et al., 2009), and different frequency components in a broadband signal, such as AE signal, may be influenced by the time-reversal operator during time reverse operations (Wang et al., 2004). Thus, it is necessary to extract the narrowband signal from AE in advance as described later. The time reversal technique is an approach meant to mitigate dispersion effects and perform SHM without baseline data. It was initially aimed at increasing lamb wave resolution by using time reversal mirrors (Fink and Prada, 2001) and focusing lamb waves at the location of damage in the time domain (Ing and Fink, 1996). According to the theoretical studies of the time reversal technique, the proposed reference signal construction principle based on time reversal for AE is shown in Figures 3 and 4. Three AE monitoring sensors were coupled on the surface of a steel plate, and an artificial AE source (Hsu-Nielson source) was simulated by a pencil-lead break (PLB) placed on the surface.

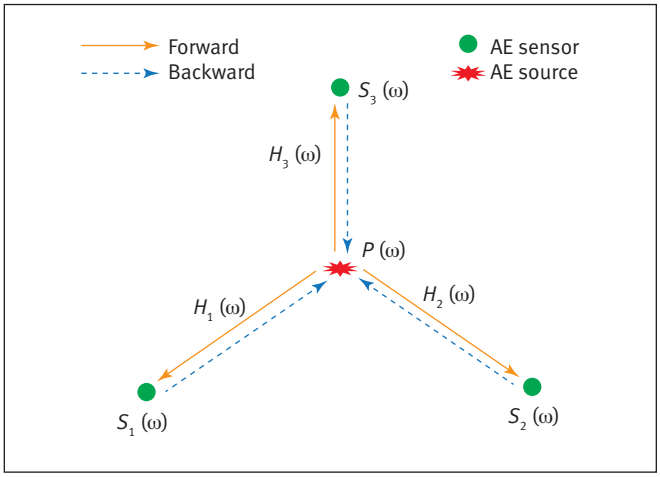

Figure 3. Illustration of AE signal focusing based on the time reversal principle with three AE sensors.

As shown in Figure 3, when an excited AE signal $P(\omega)$ is simulated on the surface of a steel plate, the response signals at three AE monitoring sensors, $S_i(\omega)$, where $(i = 1,2,3)$ can be expressed in frequency domain as:

$$S_i(\omega)=P(\omega)K(\omega)G_i(r,\omega) \quad (3)$$

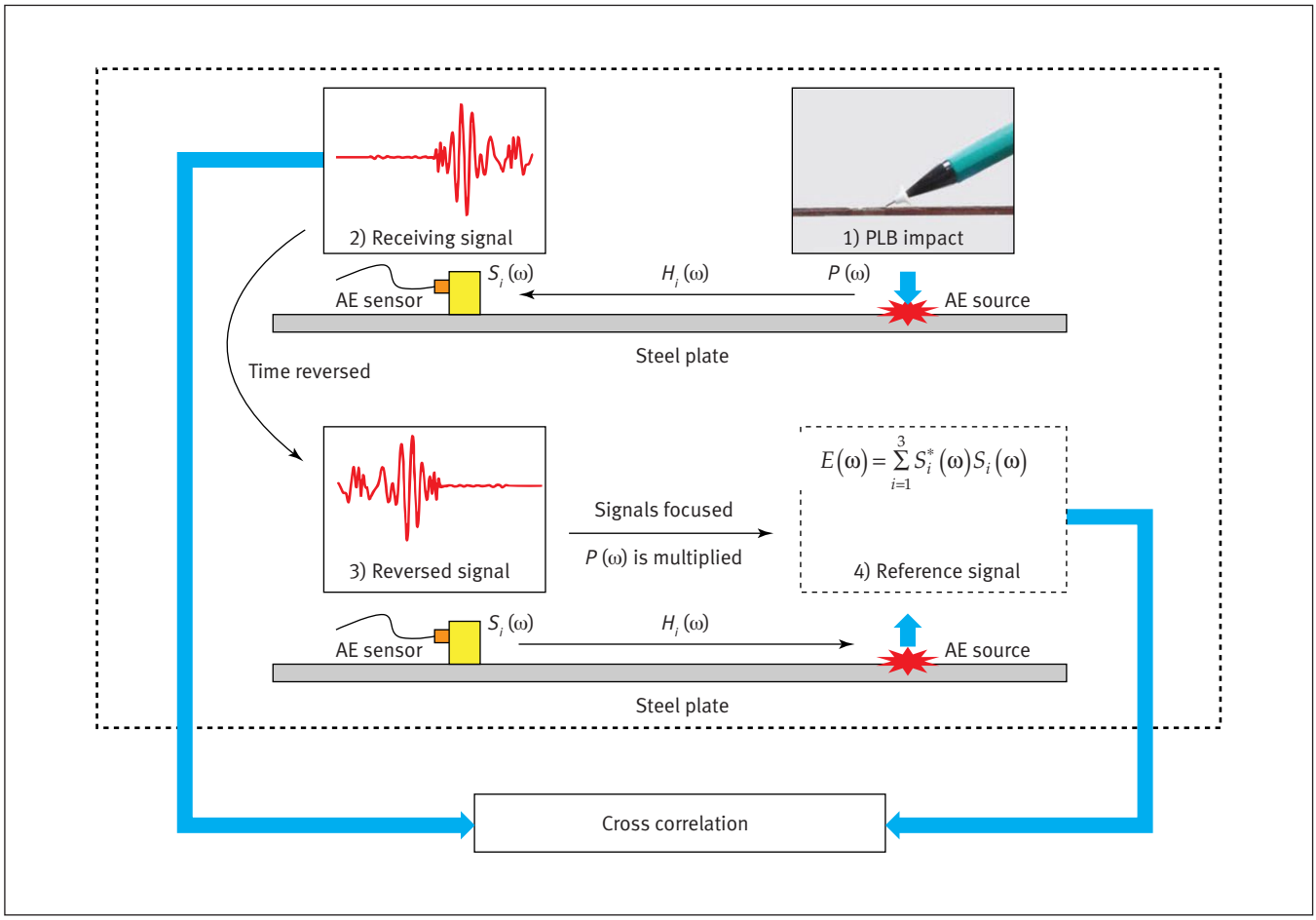

Figure 4. Illustration of the basic concept of cross correlation with AE signal in a steel plate.

where

ω is the angular frequency,

r and $G_i(r, \omega)$ for $(i = 1,2,3)$ are the propagation distance of lamb waves and the structure transfer functions of the paths between AE source and sensors, respectively,

$K(\omega)$ is the electro-mechanical efficiency coefficient of AE sensor.

$G(r,\omega)$ can be defined as

$$G(r,\omega)=A(r,\omega)e^{-jk(\omega)r} \tag{4}$$

where

$A(r, \omega)$ and $k(\omega)$ are the amplitude function and the wave number of a lamb wave mode, respectively,

j is the imaginary unit,

$e^{-jk(\omega)r}$ is a phase-delay factor.

For a particular path, $K(\omega)G_i(r, \omega)$ can be simplified as $H_i(\omega)$. Then, the response signal $S_i(\omega)$ is time reversed and re-emitted from the AE sensor to the AE source, indicating the backward propagation in Figure 3. The focused signal at the location of the PLB based on the time reversal principle can be expressed as:

$$D(\omega)=\sum_{i=1}^{3} S_i^*(\omega)H_i(\omega) \tag{5}$$

However, the focused signal, $D(\omega)$, is impossible to capture because no sensor is coupled at the location of the PLB. Furthermore, $H_i(\omega)$ is unknown. Therefore, it is more complicated to achieve the focused signal. To reconstruct the reference signal, $P(\omega)$ is multiplied by Equation 5, which is

$$\begin{aligned} E(\omega) &= D(\omega)P(\omega) \\ &= \sum_{i=1}^{3} S_i^*(\omega)H_i(\omega)P(\omega) \\ &= \sum_{i=1}^{3} P^*(\omega)H_i^*(\omega)H_i(\omega)P(\omega) \\ &= \sum_{i=1}^{3} S_i^*(\omega)S_i(\omega) \end{aligned} \tag{6}$$

In Equation 6, $E(\omega)$ can be expressed as the summation of the product of $S_i(\omega)$ and $S_i^*(\omega)$ with point wise multiplication. $D(\omega)$ is the focused signal after $P(\omega)$ is time reversed, and $E(\omega)$ can be explained as the process on which the signal is focused at the location of the PLB after $P(\omega)^*P(\omega)$ is time reversed. The process of adding terms on both sides of Equation 5 functions as an operation strategy. Because $P(\omega)^*P(\omega)$ and the original excited AE signal, $P(\omega)$, have the same frequency characteristics, no influence is introduced to the refocused signal. As $E(\omega)$ is narrowband, so $S_i(\omega)$ is processed by CWT in advance. To accomplish the cross correlation in the frequency domain, the AE signal $S_i(\omega)$ should be multiplied by the conjugate of the reference signal $E^*(\omega)$. (Note that $E^*(\omega)$ is equal to $E(\omega)$, so no additional calculation is required in cross correlation.) The basic concept of cross correlation with the AE signal in the steel plate is illustrated in Figure 4.

Experimental Investigation

Experimental Setup

As shown in Figure 5, the experimental setup consists of a pencil with 2H lead; three 150 kHz resonant frequency AE sensors with an operating frequency range of 50 to 400 kHz; three preamplifiers with gain sets at 40/60 dB; a four-channel AE signal recording card integrated in computer; a steel plate measuring 1000 mm × 1000 mm × 3 mm; and six cables. The plate was supported by a desk with both sides being free. During the experiment, three sensors were affixed with vinyl electrical tape and Nd-Fe-B magnets to the surface of the steel plate, and petroleum jelly was added between the sensors and steel plate surface for a better coupling environment. A 0.5 mm 2H pencil lead was broken on the plate's surface to simulate the AE source. AE waves were then generated and recorded by the sensors. The AE sensor outputs were preamplified by 40 dB using one of the preamplifiers. Signals were then digitized at a sampling rate of 10 MHz and stored in the computer with 2048 points.

On the surface of the steel plate, the bottom-left corner was selected as the origin of coordinates. The sensor arrangement with the coordinates of $S_1(200,90)$, $S_2(800,90)$, and $S_3(500,990)$ is shown in Figure 5. Eight different positions were chosen as the verification points for PLBs to confirm the repeatability of the experiment. The coordinates of PLB positions are shown in Table 2.

In order to ensure the stability of the experiments and reduce the errors caused by instruments or cables, a 3 mm long pencil lead was pulled out every time and a circular

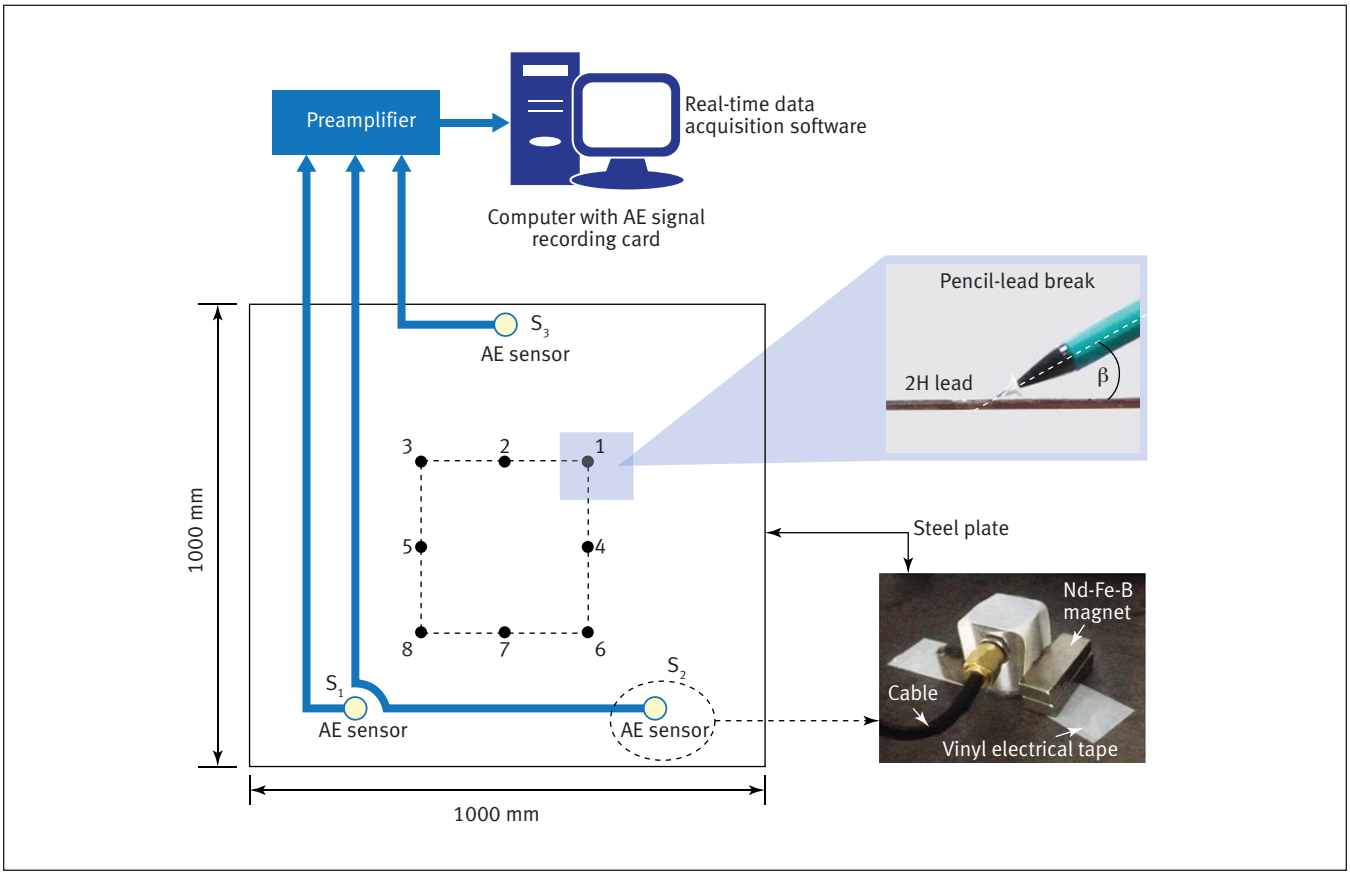

Figure 5. Illustration of experimental setup.

TABLE 2
Coordinates of PLB* positions

PLB position	#1	#2	#3	#4	#5	#6	#7	#8
x (mm)	650	500	350	650	350	650	500	350
y (mm)	690	690	690	540	540	390	390	390

* Pencil-lead break

TABLE 3
Presets of acoustic emission software applied in experiment

Threshold	Pregain	Sample rate	Pretrigger	Length of signal
40 dB	40 dB	10 MHz	25.6 μs	2048

ring was placed on the pencil lead tip so that the angle β (shown in Figure 5) formed by the lead and steel plate surface remained constant. Different angle values will cause different energy so it is necessary to ensure the consistency of β. SMA cables were chosen as the connectors between the sensors and the preamplifier to guarantee impedance matching. A commercially available software program for real-time AE data acquisition and replay was applied in the experiment. The presets of the software are provided in Table 3.

Determination of A_0 Mode Arrival Time Difference

As described in the previous section, the first step to determine arrival time difference is to extract the narrowband component from the AE signal. Figure 6 shows an AE signal received at sensor 1 when the PLB was conducted at position 1. All signals were analyzed with the same process, described as follows.

Three major wave packages with different value of energies and arrival times are visible in Figure 6, namely, wave packages 1 through 3. To determine the modes of waves and the dominant frequency of the signal, the CWT technique was used. The result is shown in Figure 7 along with the dispersion curves from Figure 2. The obvious zone denotes the component with the highest energy. The intersection of the two dotted lines in Figure 7 represents the dominant frequency component with a frequency of 131.8 kHz. The CWT result matches well with the dispersion curve. As shown in Figure 7, wave package 1 is the S_0 mode and wave package 3 is the A_0 mode. Wave package 2 arrives before the A_0 mode with a frequency component around 300 kHz and is considered the shear horizontal (SH) mode according to the analysis (Kaphle, 2012b; Geng, 2006). The SH mode is another type of guided wave mode that propagates in plate-like structures. It should be noted that the initial time (PLB time) of the AE waves is not at the zero point (Figure 7), so the reflection signal from the plate edges arrives after 200 μs (the length of the storage signal is 2048 points and the time interval is 0.1 μs), even for the fast S_0 mode. The possible multiple scattering of signals due to the existence of sensors is also considered as a negligible effect due to the large sensor-to-source distance, which is ignored during the analysis of signals. In conclusion, wave packages 1 through 3 represent the direct waves of S_0 mode, SH mode, and A_0 mode, respectively.

Figure 8 shows the AE signals before and after extraction, based on CWT. Figures 8a and 8b show the original AE signal in time domain and the normalized frequency spectrum of

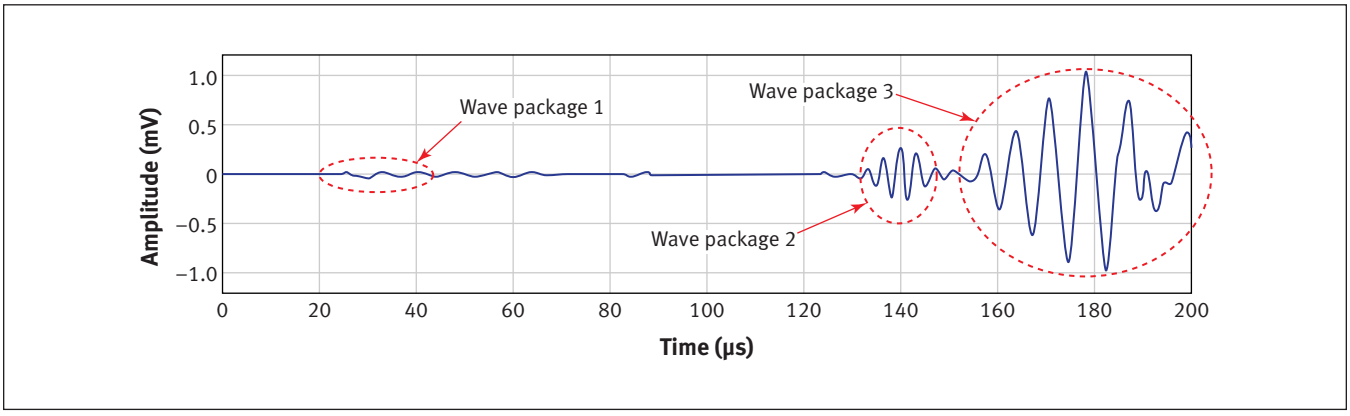

Figure 6. An AE signal received at sensor 1 when conducted PLB at position 1.

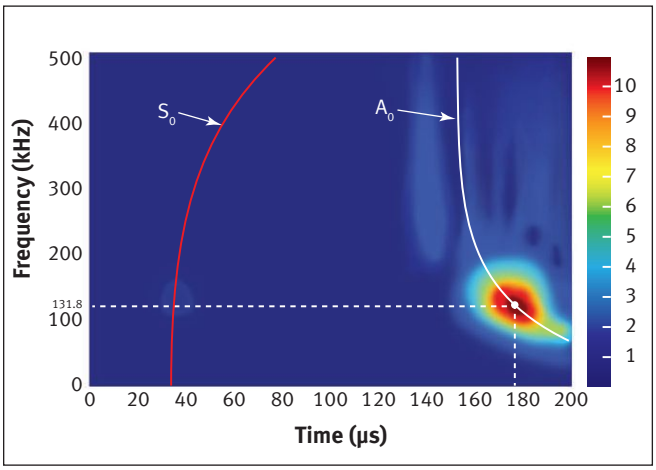

Figure 7. Time-frequency spectrogram of AE signal.

this original AE signal using FFT, respectively. The frequency of the signal falls off above 400 kHz because the AE sensor operates at a frequency range of 50 to 400 kHz. The original signal has two main frequency components, 131.8 kHz and around 300 kHz, which can be seen in Figure 8b. However, the 131.8 kHz component has a higher value of energy than the 300 kHz component. The 131.8 kHz component is the dominant frequency component of the AE signal. Figure 8c shows the wavelet coefficient signal, extracted from the original AE signal shown in Figure 8a at a frequency of 131.8 kHz, based on the CWT technique. Figure 8d shows the normalized frequency spectrum of the extracted wavelet coefficient signal using FFT. By comparing the signals and the frequency spectrums before and after the extraction, we can see that the high-frequency component (SH mode) has been filtered out. The two signals have the same dominant frequency, 131.8 kHz. Moreover, after the signal extraction, the band of the signal becomes narrow. As a narrowband signal gives a better result than a wideband signal in signal focusing processes based on the time reversal principle, the signal shown in Figure 8c was used to construct the reference signal. Figure 9 shows the constructed reference signal with the extracted wavelet coefficient signal from the original AE sensor outputs.

Figure 10 shows the process of determining the trigger mode by using the signals received by the data acquisition software. In the data acquisition process, the pretrigger was set at 25.6 μs and the threshold was 40 dB. In the software, 40 dB equals to 0.01 V. For all sensors' outputs, AE waves cross the threshold line for the first time at 25.6 μs, indicating that the arrival time is 25.6 μs. However, the arrival times from different sensors should be different because of different propagating paths from the PLB position to the AE sensors. The difference was introduced by the data acquisition

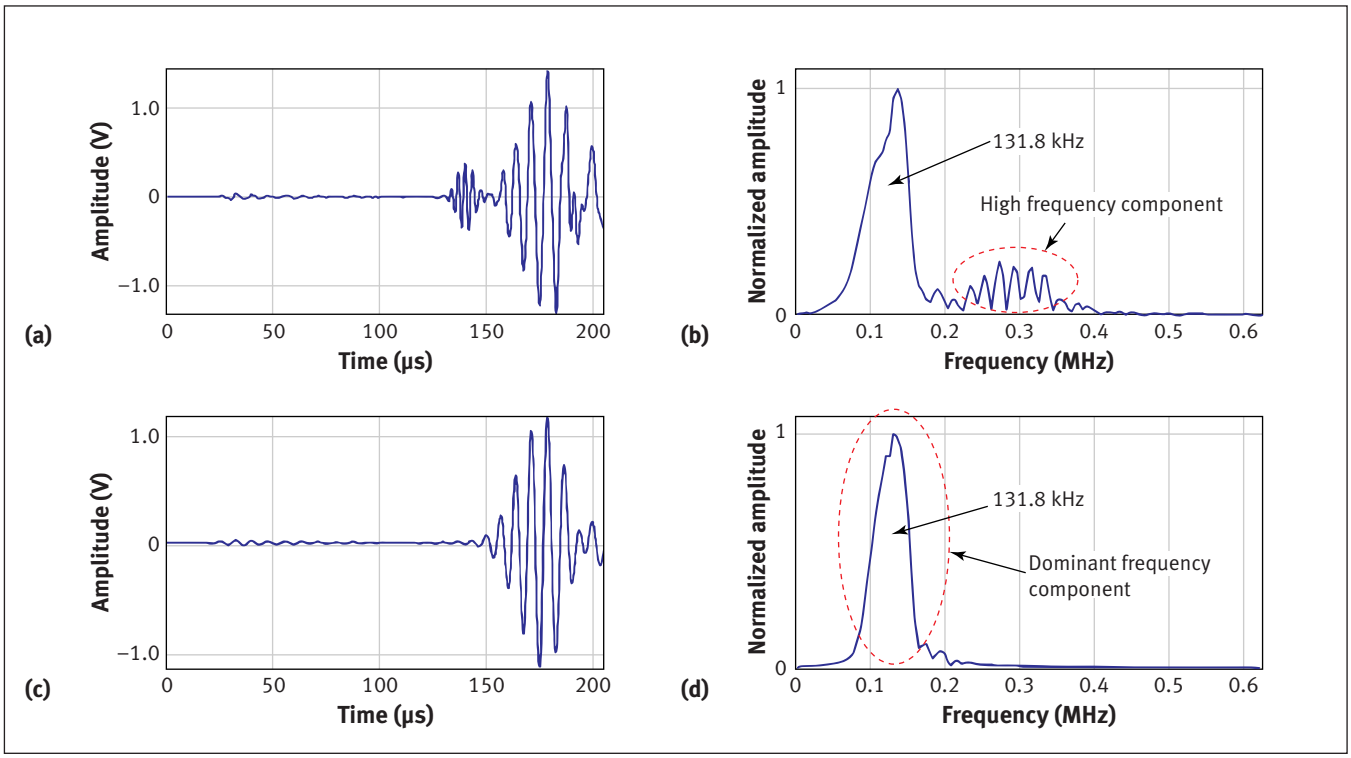

Figure 8. Comparison of original AE signal (broadband) and the extracted AE signal (narrowband): (a) original AE signal in time domain; (b) normalized frequency spectrum of original AE signal using FFT; (c) wavelet coefficient signal extracted from original AE signal at 131.8 kHz based on CWT method; (d) normalized frequency spectrum of the extracted wavelet coefficient signal by FFT.

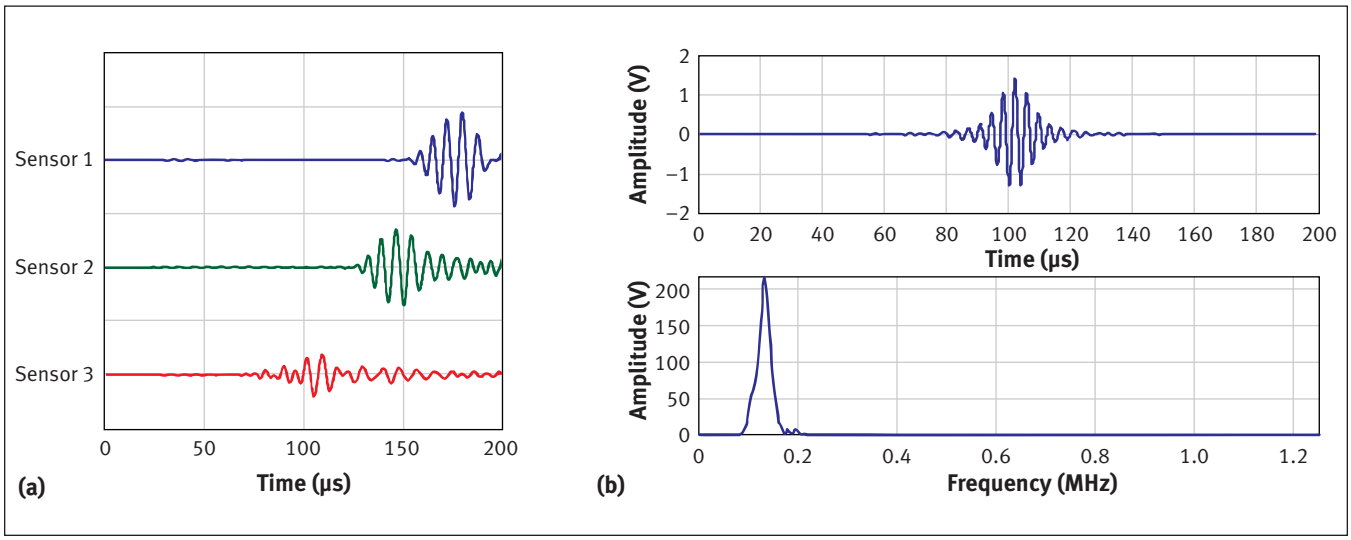

Figure 9. Reference signal construction: (a) extracted wavelet coefficient signals from three AE sensor outputs when PLB was conducted at position 1; (b) the reference signal (above) and its frequency spectrum (below).

software measurement. The principle of introducing differences by using the software measurement is illustrated in Figure 11. Run time represents the starting time of the software, and PLB time represents the time of breaking the pencil lead. Nevertheless, it is impossible to record run time and PLB time. When the waves were captured by the software, waves from the three paths firstly crossed the threshold line and were all set at 25.6 μs, as shown in Figure 11b. So the time delay of the A_0 mode, as displayed in the software, is not the actual arrival time difference of the A_0 mode (Δt_{A0}) but the relative arrival time difference of the A_0 mode (Δt). This phenomenon indicates that the actual arrival time difference of the A_0 mode (Δt_{A0}) can be obtained by adding Δt_{S0} to Δt. Because the S_0 mode shows great characteristics, such as a nondispersive characteristic in thin plates, and Δt is processed by cross correlating AE signals with the reference signal based on the time reversal principle, Δt_{A0} shows more accuracy without having dispersion. Table 4 shows the arrival time differences obtained from the first threshold-crossing technique and those obtained from the cross-correlation technique.

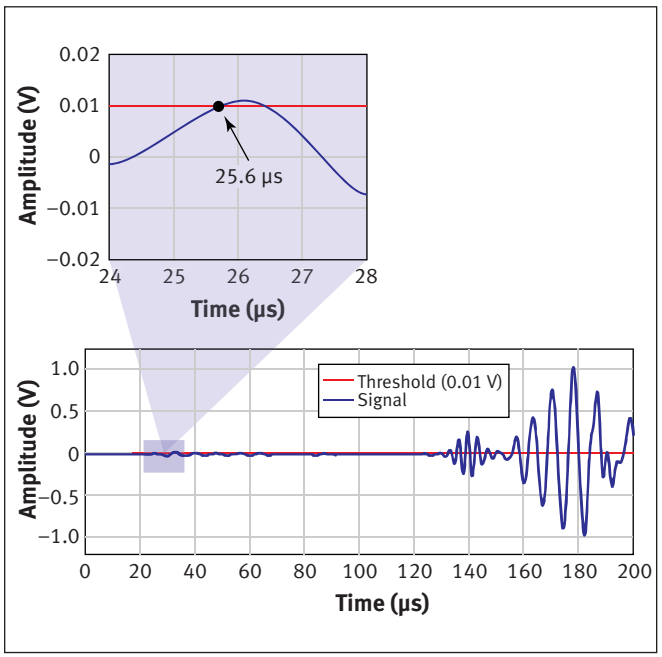

Figure 10. Pretrigger mode determination with the received signals from the AE software.

Localization Result Analysis

The AE source localization with arrival time difference was performed through programmed MATLAB codes. The velocities used in the localization algorithm were the theoretical group velocities obtained from the dispersion curves shown in Figure 2. It has been shown through other research that the group velocity of AE waves is frequency dependent and may vary with different tests. However, this was not the major error to overcome in this research. For every testing point, the velocities were determined by the dominant frequencies from dispersion curves based on CWT. For A_0 mode localization, the errors were minimized by dispersion compensation based on the time reversal principle. Nevertheless, errors will be

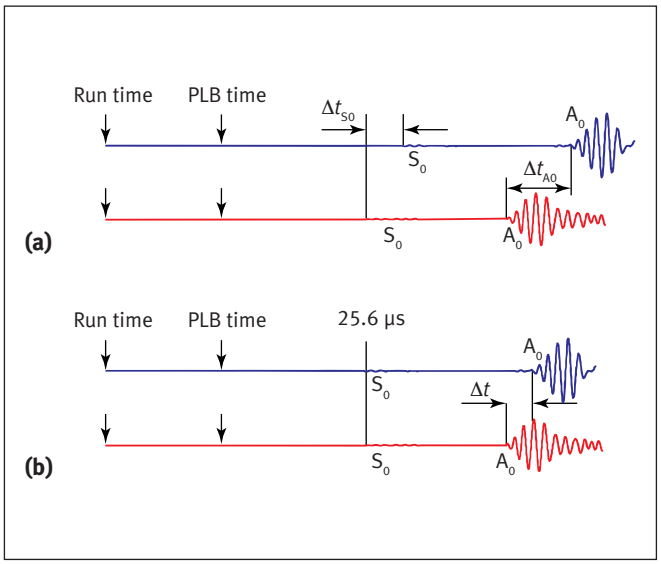

Figure 11. The principle of introducing difference by measurement from software program for AE data acquisition and replay: (a) the actual arrival time of different modes: and (b) the relative arrival time of different modes captured with the first threshold-crossing technique by the software program.

inevitably introduced in the localization results, which should not be ignored. The localization result is shown in Figure 12, and the position of sensor 1 is chosen as the origin of the coordinate.

Figure 12 shows the localization results by the first threshold-crossing technique and by the proposed technique. Among eight verification points, the localization results, obtained with the proposed technique, match well with the actual positions of the PLB. Localization errors have also been analyzed. The radius error described in Figure 12b is the distance from the coordinates of the located points to the actual PLB coordinates. The relative error is obtained by dividing the radius error by the largest distance among three sensors. As described previously, the distance from sensor 1 to sensor 3 is the largest distance, 948.7 mm. According to the localization results obtained with the traditional first threshold-crossing technique, the maximum radius error is 44.5 mm at position 1 with a relative error of 4.69%, and the minimum radius error is 7.0 mm at position 8 with a relative error of 0.74%. According to the localization results obtained with the proposed technique, the maximum radius error is 9.3 mm at position 5 with a relative error of 0.98%, and the minimum radius error is 5.5 mm at position 4 with a relative error of 0.56%.

Conclusion

In this paper, we have combined the cross-correlation technique with the time reversal principle, and have proposed a novel approach to identify the arrival time difference of the A_0 mode in AE source localization.

This study is focused on the determination of the arrival time difference of the A_0 mode in AE source localization. The A_0 mode can travel a long distance with high energy, indicating that the A_0 mode has a great potential to monitor large plate-like structures. However, as the A_0 mode shows serious dispersive characteristics, it is not easy to obtain the arrival time difference of the A_0 mode (Δt_{A0}) with a satisfying accuracy. In this paper, the proposed technique is used to obtain Δt_{A0}, and results have shown that the experimental positions localized with the proposed technique matched well with the actual PLB positions. The localization accuracy is good and the maximum relative error is 0.98%. The reason is that, while determining Δt_{A0} in the process of localization, errors were minimized due to narrowband signal extraction with CWT and dispersion compensation of the time-reversal principle. It is necessary to localize the AE source with A_0 mode in large plate-like structures, because the A_0 mode has high energy and long traveling ability. Thus, this paper has provided an optional technique to localize AE sources with the A_0 mode, which is of significant meaning.

TABLE 4
Arrival time differences of A_0 mode obtained by the proposed method

PLB position	Δt_{S0} (µs)		Δt (µs)		Δt_{A0} (µs)	
	Δt_{12}	Δt_{13}	Δt_{12}	Δt_{13}	Δt_{12}	Δt_{13}
#1	−17.75	−72.25	−27.60	−69.30	−45.35	−141.55
#2	2.50	−62.50	−0.40	−74.00	2.10	−136.50
#3	27.50	−49.25	21.60	47.30	49.10	−96.55
#4	−24.05	−27.50	−30.60	32.30	−54.65	59.80
#5	29.45	−4.25	29.50	1.00	58.95	−3.25
#6	−35.75	15.75	−39.20	8.40	−74.95	24.15
#7	2.75	36.75	−0.60	25.90	2.15	62.65
#8	39.75	55.50	33.30	41.00	73.05	96.50

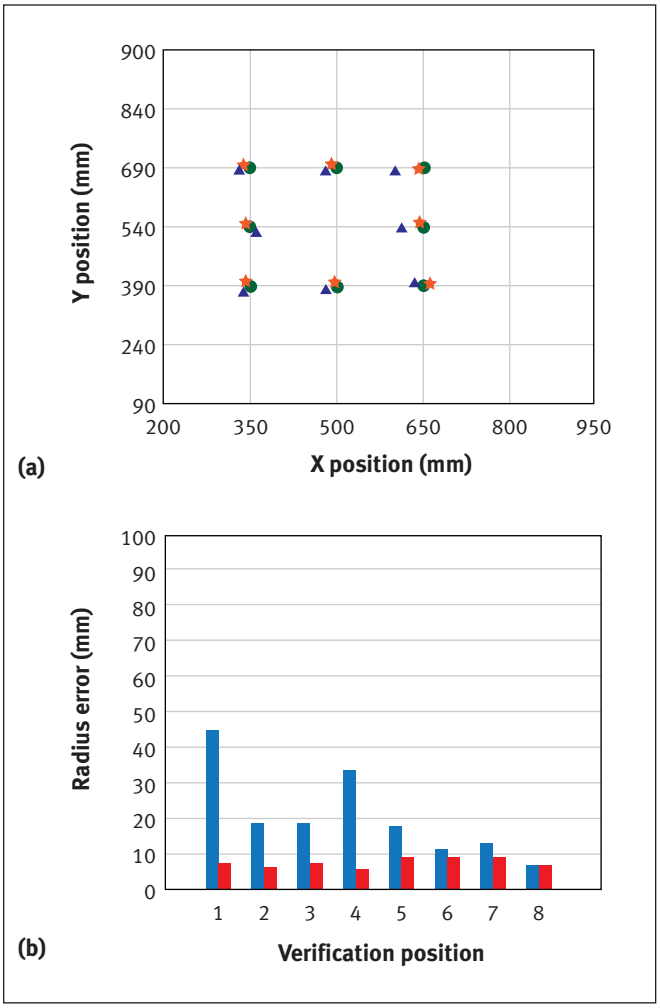

Figure 12. Localization results analysis: (a) ● represents the actual PLB position, ▲ represents the results localized by the first threshold-crossing technique, and ★ represents the results localized by the proposed method; (b) radius errors from the first threshold-crossing technique (shown in blue) and radius errors from the proposed method (shown in red).

In this paper we compared the proposed technique with the first threshold-crossing technique, and the results were good. More works concerning localizing AE sources with the experimental velocity and comparing them to other AE source-location schemes using the proposed technique are being studied.

ACKNOWLEDGMENTS

This work was supported by the National Natural Science Foundation of China (Grant Nos. 51475012, 11272021, 11772014, and 51235001), the Scientific Research Project of Beijing Educational Committee (Grant No. KM201010005003), and the Importation and Development of High-Caliber Talents Project of Beijing Municipal Institutions (Grant No. CIT&TCD201304048).

REFERENCES

Aljet, D., A. Chong, S. Wilcox, and K. Holford, 2012, "Acoustic Emission Source Location On a Large Plate-Like Structures Using a Local Triangular Sensor Array," *Mechanical Systems and Signal Processing*, Vol. 30, pp. 91–102.

Barthorpe, R., K. Worden, M.T.H. Sultan, M. Eaton, R. Pullin, and K.M. Holford, 2012, "The Effect of Attenuation On the Identification of Impact Damage in CFRP Laminates," *AIP Conference Proceedings*, Vol. 1, pp. 698–706.

Chen, C., Y. Li, and F.G. Yuan, 2011, "Impact And Damage Location Detection On Plate-Like Structures Using Time-Reversal Method," *Structural Health Monitoring 2011: Condition-based Maintenance and Intelligent Structures*, Vol. 1, pp. 274–281.

Chen, C.L., Y.L. Li, and F.G. Yuan, 2012, "Impact Source Identification in Finite Isotropic Plates Using a Time-Reversal Method: Experimental Study," *Smart Materials and Structures*, Vol. 21, No. 10, pp. 1052–1053.

Ciampa, F., and M. Meo, 2010, "A New Algorithm For Acoustic Emission Localization and Flexural Group Velocity Determination In Anisotropic Structures," *Composites Part A: Applied Science and Manufacturing*, Vol. 41, No. 12, pp. 1777–1786.

Ciampa, F., and M. Meo, 2011, "Acoustic Emission Localization in Complex Dissipative Anisotropic Structures Using a One-Channel Reciprocal Time Reversal Method," *Journal of the Acoustical Society of America*, Vol. 130, No. 1, pp. 168–175.

Draeger, C., and M. Fink, 1999, "One-Channel Time-Reversal In Chaotic Cavities: Theoretical Limits," *Journal of the Acoustical Society of America*, Vol. 105, No. 2, pp. 611–617.

Draeger, C., J.C. Aime, and M. Fink, 1999, "One-Channel Time-Reversal in Chaotic Cavities: Experimental Results," *Journal of the Acoustical Society of America*, Vol. 105, No. 2, pp. 618–625.

Ernst, R., and J. Dual, 2014, "Acoustic Emission Localization In Beams Based On Time Reversed Dispersion," *Ultrasonics*, Vol. 54, No. 6, pp. 1522–1533.

Fink, M., and C. Prada, 2001, "Acoustic Time-Reversal Mirrors," *Inverse Problems*, Vol. 17, No. 1, pp. R1–R38.

Geng R.S., 2006, "Modern Acoustic Emission Technique and Its Application in Aviation Industry," *Ultrasonics*, Vol. 44, pp. E1025–29.

Grondel, S., C. Delebarre, J. Assaad, J.P. Dupuis, and L. Reithler, 2002, "Fatigue Crack Monitoring of Riveted Aluminum Strap Joints by Lamb Wave Analysis and Acoustic Emission Measurement Techniques," *NDT & E International*, Vol. 35, No. 3., pp. 137–146.

Han, Z.Y., H.Y. Luo, J.W. Cao, and H.W. Wang, 2011, "Acoustic Emission During Fatigue Crack Propagation In a Micro-Alloyed Steel and Welds," *School of Materials Science and Engineering*, No. 528, pp. 7751–7756.

Harb, M.S., and F.G. Yuan, 2015, "A Rapid, Fully Non-Contact, Hybrid System for Generating Lamb Wave Dispersion Curves," *Ultrasonics*, Vol. 61, pp. 62–70.

He, J., and F.G. Yuan, 2016, "Lamb Wave-Based Subwavelength Damage Imaging Using the DORT-MUSIC Technique In Metallic Plates," *Structural Health Monitoring*, Vol. 15, No. 1, pp. 65–80.

He, J., and F.G. Yuan, 2017, "Lamb-Wave-Based Two-Dimensional Areal Scan Damage Imaging Using Reverse-Time Migration With a Normalized Zero-Lag Cross-Correlation Imaging Condition," *Structural Health Monitoring*, Vol. 16, No. 4, pp. 444–457.

Ing, R. K., and M. Fink, 1996, "Time Recompression of Dispersive Lamb Waves Using a Time Reversal Mirror-Application to Flaw Detection in Thin Plates," *IEEE Ultrasonics Symposium Proceedings*, Vol. 1-2, pp. 659–63.

Ing, R.K., and M. Fink, 1998, "Time-Reversed Lamb Waves," *IEEE Transactions on Ultrasonics, Ferroelectrics, and Frequency Control*, Vol. 45, No. 4, pp. 1032–1043.

Kaphle, M., 2012a, "Analysis of Acoustic Emission Data for Accurate Damage Assessment for Structural Health Monitoring Applications," Queensland University of Technology, PhD Dissertation, Ch. 2.

Kaphle, M., 2012b, "Analysis of Acoustic Emission Data for Accurate Damage Assessment for Structural Health Monitoring Applications," Queensland University of Technology, PhD Dissertation, Ch. 3.

Kim, J.H., Y.Y. Kim, Y. Park, and C.G. Kim, 2015, "Low-Velocity Impact Localization In a Stiffened Composite Panel Using a Normalized Cross-Correlation Method," *Smart Materials and Structures*, Vol. 24, No. 4, p. 045036.

Kishi, T., M. Enoki and H. Tsuda, 1991, "Interface and Strength in Ceramic Matrix Composites," *Materials Science and Engineering: A*, Vol. 143, Nos. 1–2, pp. 103–110.

Kishimoto, K., H. Inoue, M. Hamada, and T. Shibuya, 1995, "Time Frequency Analysis of Dispersive Waves By Means Of Wavelet Transform," *Journal of Applied Mechanics*-trans. ASME, Vol. 62, No. 4, pp. 841–846.

Kundu, T., 2014, "Acoustic Source Localization," *Ultrasonics*, Vol. 54, No. 1, pp. 25–38.

Li, Q.F., Y. Wang, R.M. Liu, W. Gu, and F. Ao, 2015, "Ultrasonic Computed Tomography Imaging Method Of Concrete Materials Based on Simulated Annealing Genetic Algorithm," *Trans. Nanjing University of Aeronautics and Astronautics*, Vol. 32, No. 3, pp. 341–347.

Liu, S.T., L. Liu, and F.G. Yuan, 2011, "Defect Imaging Using Time-Reversal Technique," *Proceedings SPIE Smart Materials + Nondestructive Evaluation and Health Monitoring*, Vol. 7981, p. 79811R.

Liu, Z.H., H.T. Yu, C.F. He, and B. Wu, 2013a, "Delamination Damage Detection Of Laminated Composite Beams Using Air-Coupled Ultrasonic Transducers," *Science China: Physics, Mechanics and Astronomy*, Vol. 56, No. 7, pp. 1269–1279.

Liu, Z.H., F.X. Yu, R. Wei, C.F. He, and B. Wu, 2013b, "Image Fusion Based On Single-Frequency Guided Wave Mode Signals for Structural Health Monitoring in Composite Plates," *Materials Evaluation*, Vol. 71, No. 12, pp. 1434–1443.

Liu, Z.H., Q.L. Xu, Y. Gong, C.F. He, and B. Wu, 2014, "A New Multi-channel Time Reversal Focusing Method for Circumferential Lamb Waves and Its Applications for Defect Detection in Thick-Walled Pipe With Large-Diameter," *Ultrasonics*, Vol. 54, pp. 1967–1976.

Liu, Z.H., H.T. Yu, J.W. Fan, C.F. He, and B. Wu, 2015a, "Baseline-Free Delamination Inspection in Composite Plates by Synthesizing Non-Contact Air-Coupled Lamb Wave Scan Method and Virtual Time Reversal Algorithm," *Smart Materials and Structures*, Vol. 24, No. 4, p. 045014.

Liu, Z.H., J.W. Fan, Y.N. Hu, C.F. He, and B. Wu, 2015b, "Torsional Mode Magnetostrictive Patch Transducer Array Employing a Modified Planar Solenoid Array Coil for Pipe Inspection," *NDT & E International*, Vol. 69, pp. 9–15.

Mohd, S., K.M. Holford, and R. Pullin, 2014, "Continuous Wavelet Transform Analysis and Modal Location Analysis Acoustic Emission Source Location For Nuclear Piping Growth Monitoring," *AIP Conference Proceedings*, Vol. 1584, No. 61, pp. 61–68.

Mostafapour, A., and S. Davoodi, 2015, "Continuous Leakage Location In Noisy Environment Using Modal and Wavelet Analysis With One AE Sensor," *Ultrasonics*, Vol. 62, pp. 305–311.

Mustapha, S., Y. Lu, J.C. Li, and L. Ye, 2014, "Damage Detection in Rebar-Reinforced Concrete Beams Base On Time Reversal of Guided Waves," *Structural Health Monitoring*, Vol. 13, No. 4, pp. 347–358.

Niri, E.D., and Salamone S., 2012, "A Probabilistic Framework for Acoustic Emission Source Localization in Plate-Like Structures," *Smart Materials and Structures*, Vol. 21, No. 3, p. 035009.

Park, H.W., S.B. Kim, and H. Sohn, 2009, "Understanding a Time Reversal Process in Lamb Wave Propagation," *Wave Motion*, Vol. 46, No. 7, pp. 451–467.

Poggi, V., D. Fah, and D. Giardini, 2013, "Time-Frequency-Wavenumber Analysis of Surface Waves Using the Continuous Wavelet Transform," *Pure and Applied Geophysics*, Vol. 170, pp. 319–335.

Pullin, R., D.C. Carter, and M. Holford, 1999, "Damage Assessment in Steel Bridges," *Key Engineering Materials*, Vol. 167, pp. 335–342.

Sedlak, P., Y. Hirose, and M. Enoki, 2013, "Acoustic Emission Localization In Thin Multi-Layer Plates Using First-Arrival Determination," *Mechanical Systems and Signal Processing*, Vol. 36, No. 2, pp. 636–649.

Sohn, H., H.W. Park, K.H. Law, and C.R. Farrar, 2007, "Damage Detection in Composite Plates by Using An Enhanced Time Reversal Method," *Journal of Aerospace Engineering*, Vol. 20, No. 3, pp. 141–151.

Tanter, M., J.L. Thomas, and M. Fink, 2000, "Time Reversal and the Inverse Filter," *Journal of the Acoustical Society of America*, Vol. 108, No. 1, pp. 223–34.

Wang, C.H., J.T. Rose, and F.K. Chang, 2004, "A Synthetic Time-Reversal Imaging Method for Structural Health Monitoring," *Smart Materials and Structures*, Vol. 13, No. 2, pp. 415–423.

Watkins, R., and R. Jha, 2012, "A Modified Time Reversal Method For Lamb Wave Based Diagnostics of Composite Structures," *Mechanical Systems and Signal Processing*, Vol. 31, pp. 345–354.

Wevers, M., 1997, "Listening To The Sound of Materials: Acoustic Emission For The Analysis Of Material Behavior," *NDT & E International*, Vol. 30, No. 2, pp. 99–106.

Xiao, D.X, T. He, Q. Pan, X.D. Liu, J. Wang, and Y.C. Shan, 2014, "A Novel Acoustic Emission Beamforming Method With Two Uniform Linear Arrays On Plate-Like Structures," *Ultrasonics*, Vol. 54, No. 2, pp. 737–45.

Zarate, B. A., A. Pollock, S. Momeni, and O. Ley, 2015, "Structural Health Monitoring Of Liquid-Filled Tanks: A Bayesian Approach For Location Of Acoustic Emission Sources," *Smart Materials and Structures*, Vol. 24, No. 1, p. 015017.

Zhong, Y.T., S.F. Yuan, and L. Qiu, 2015, "Multi-Impact Source Localization On Aircraft Composite Structure Using Uniform Linear PZT Sensors Array," *Structure and Infrastructure Engineering*, Vol. 11, No. 3, pp. 310–320.

Ziola, S.M., and M.R. Gorman, 1991, "Source Location in Thin Plates Using Cross-Correlation," *Journal of the Acoustic Society of America*, Vol. 90, No. 5, pp. 2551–2556.

Zitto, M. E., R. Piotrkowski, A. Gallego, F. Sagasta, and A. Benavent-Climent, 2015, "Damage Assessed by Wavelet Scale Bands and B-Value in Dynamical Tests of a Reinforced Concrete Slab Monitored With Acoustic Emission," *Mechanical Systems and Signal Processing*, Vols. 60–61, pp. 75–89.